Preparation and characterization of potato starch/bentonite organophylized by SDS

N. Amrouni, A. Meziane, and A. Boussaid*

Laboratoire de Recherche sur les Macromolécules
University Abou Beker Belkaid Tlemcen, BP 119, 13000 Tlemcen, Algeria,
**e-mail: a_bousaiddz@yahoo.fr*
Tel: +213664051808

Received 27 December 2023; accepted 10 August 2024

This study focuses on the development of nanocomposite films using potato starch via a casting technique. Glycerol was incorporated as a plasticizer, while Sodium Dodecyl Sulfate (SDS)-modified bentonite acted as reinforcement. Various analytical methods, including Fourier transform infrared (FTIR), X-ray diffraction (XRD), Thermogravimetric analysis (TGA), UV/vis spectroscopy, Electron microscopy (SEM), and Optical microscopy (MOP), were utilized to assess the material properties. Different concentrations of SDS, below, at, and above the critical micelle concentration (CMC), were investigated. The findings suggest that films containing higher SDS levels demonstrate enhancements in both physical and chemical characteristics. XRD assessments reveal that films with SDS concentrations surpassing the CMC level display homogeneity, indicating effective intercalation or exfoliation processes. This compatibility of the biofilm components is further evidenced through FTIR, SEM, and MOP. Moreover, the introduction of SDS significantly improves the film's biodegradability, as confirmed by thermogravimetric analysis.

Keywords: Biofilms; starch; bentonit; SDS surfactant; compatibility.

DOI: https://doi.org/10.31349/RevMexFis.71.021001

1. Introduction

While petroleum-based plastic products have become integral to various aspects of daily life, their poor degradability poses a significant environmental threat [1–3]. Consequently, considerable research efforts are being directed towards tackling the challenges of plastic waste and advocating for the large-scale adoption of eco-friendly alternatives. Polysaccharides, like starch derived from potatoes or rice, emerge as promising substitutes for traditional plastics due to their abundance, renewability, and cost-effectiveness [4, 5]. Although polysaccharide-based plastics hold promise, they face inherent physical and chemical limitations, prompting researchers to explore composite materials to improve their properties [6–8]. Indeed, some studies have shown that the addition of carefully chosen components significantly improves the physicochemical and mechanical properties of these biofilms. For example,the incorporation of glycerol, functioning as a plasticizer, bestows flexibility upon the material by intercalating amidst starch molecules, resulting in more supple films [9–11]. Additionally, the integration of bentonite clay notably bolsters mechanical strength owing to its distinctive chemical composition and structure [12, 13]. Bentonite clay typically comprises multiple layers with interlayer spaces hosting regularly packed ions. Under conducive conditions, the interaction between bentonite and charged molecules prompts intercalation and, in certain instances, exfoliation, thereby augmenting the uniformity and mechanical prowess of the composite [14, 15].

On the other hand, the organophilisation of bentonite, achieved through modification with organic molecules like surfactants, seeks to impart hydrophobic properties to the bentonite, thereby easing its integration into organic polymers. In addition to enhancing dispersion and mechanical reinforcement, this versatile technique enables efficient adsorption and removal of contaminants. Moreover, the expanded application range resulting from organophilisation greatly enhances the performance of composite materials, benefiting various industrial sectors.

This investigation zeroes in on enhancing starch/glycerol-based films reinforced with bentonite and Sodium Dodecyl Sulfate (SDS) surfactant, renowned for its beneficial attributes. Specifically, we delve into the impact of SDS concentration, scrutinizing three concentrations-higher, equivalent, and lower than its critical micellar concentration analyzing the ensuing outcomes.

2. Materials and methods

2.1. Materials

The chemicals used in our experiments are commercially available products. The potato-starch (Stch), a white fine powder with $10\,wt\,\%$ moisture content containing $35 - 15\,wt\,\%$ amylose and $65 - 85\,wt\,\%$ amylopectin, was purchased from Tuoketuohua Starch Company (Neimeng, China). The Bentonite (Bt) and glycerol were obtained from Sigma-Aldrich Co. The structural formula of the anionic surfactant, sodium dodecyl sulphate (SDS) is

($C_{12}H_{25}SO_4^-$+Na^+), was purchased from FlukaChemical. All chemicals used are pure grade.

2.2. Experimental techniques and characterization

2.2.1. X-ray diffraction analysis

X-ray diffraction was conducted using a Mini Flex 600 X-ray diffractometer to measure inter-reticular distance and determine the exfoliation rate. The following conditions were employed: F.F tube 40 kV and 15 mA. Films were exposed to Cu radiation at a wavelength of 1.54 nm and scanned over a $2\,\theta$ diffraction angle interval of $2 - 30°$ with a scan speed of $10°$/min.

2.2.2. Transform infrared (FTIR) spectra

FTIR spectra of the films were recorded using an Agilent Cary 640 FTIR spectrophotometer across the range of 400-4000 cm^{-1} employing a transmission method.

2.2.3. Thermal properties

TGA-DTA analysis of films was performed using a Linseis TGA PT1600 differential thermal analyzer. Samples weighing 9-10 mg were heated to $600°$C at a rate of $10°$/min under a nitrogen atmosphere. Weight loss was measured as a function of temperature.

2.2.4. Opacity

Opacity values of the films were determined using an Analytikjena, Specord 200 plus UV/VIS spectrophotometer. Rectangular pieces of films were placed in the sample compartment of the spectrophotometer. An empty compartment served as a reference in the measurements. Absorbance spectra of the films were recorded over the range of 200 to 800 nm, and opacity values were calculated using the equation:

$$\text{Opacity} = \text{Abs}(600)/X, \tag{1}$$

where Abs 600 is the absorbance value at 600 nm and X (mm) is the film thickness.

2.2.5. Scanning electron microscope

The surface morphology of $Stch/Bt$ and $Stch/SDS/Bt$ films was examined using a scanning electron microscope performed with a VEGA3 TESCAN. Computations were made using Microcal Origin.

2.2.6. Optical microscope

Optical microscopy (MOP) analysis was conducted using an OLYMPUS BX41.

2.2.7. Measurement of film thickness

Film thickness was measured using an electronic outside micrometer with a sensitivity of 0.001 mm. The average of ten measurements for each thickness was considered in this work.

2.3. Film preparation

Four solutions of bentonite with a concentration of 0.125 g per 45 g of water were prepared using magnetic stirring for a duration of 24 hours, followed by sonication for one hour. To achieve three different concentrations, SDS was incorporated into the previously prepared bentonite solutions, resulting in higher (0.0035 g/ml), lower (0.0018 g/ml), and equal (0.0025 g/ml) concentrations compared to the CMC. These three solutions were further stirred for an additional 24 hours. Additionally, potato starch (2.5 g) and glycerol (0.75 g) were added to each of the three previously prepared solutions, which were subsequently subjected to mechanical agitation for 15 minutes at a temperature of $80°$C. A fourth control solution was prepared without the addition of SDS using the same methodology. All solutions, prepared at a pH of 5.5, were poured into Petri dishes and dried for a week at room temperature. The resulting dry films were then removed from the molds.

3. Results and discussions

3.1. Representation of the different compositions of the solutions

The images presented in Fig. 1a) illustrate that the film, in the absence of SDS, exhibits fragility and lacks visual appeal. Films produced at SDS concentrations equal to or below its Critical Micelle Concentration (CMC) are prone to deterioration under storage conditions, as indicated by the presence of spots on the film surface. Conversely, when SDS concentration surpasses the CMC threshold [as illustrated in Fig. 1c)], the film achieves its optimal condition.

TABLE I. Representation of the different compositions of the solutions prepared for the films produced.

FILMS COMPOSITION	$Bt\,(g)$	$SDS\,(g)$	$Starch\,(g)$
$Bt/Stch$	0.125	-	2.5
$Bt/SDS_{<CMC}$	0.125	0.085	-
$Bt/SDS_{=CMC}$	0.125	0.1165	-
$Bt/SDS_{>CMC}$	0.125	0.1581	-
$Bt/SDS_{<CMC}/Stch$	0.125	0.085	2.5
$Bt/SDS_{=CMC}/Stch$	0.125	0.1165	2.5
$Bt/SDS_{>CMC}/Stch$	0.125	0.1581	2.5

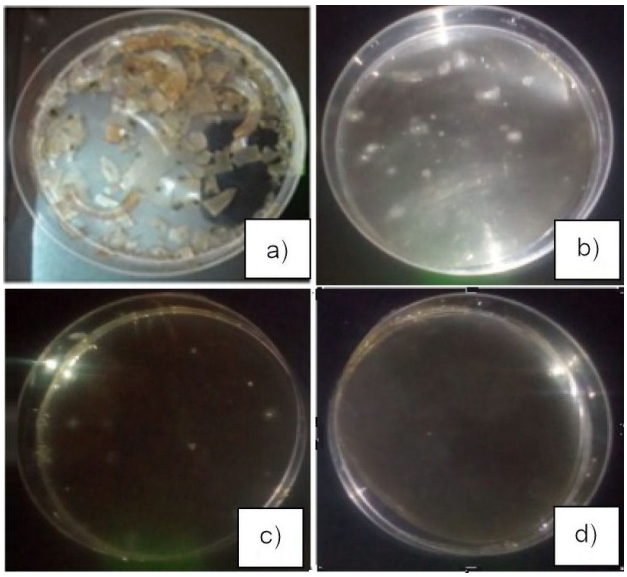

FIGURE 1. Photographs of the different films obtained a) $Bt/Stch$, b) $Bt/SDS_{<CMC}/Stch$, c) $Bt/SDS_{=CMC}/Stch$ and d) $Bt/SDS_{>CMC}/Stch$.

3.2. FTIR analysis

Figure 2 showcases the FTIR spectra of Bt, SDS, and the organo-bentonite Bt/SDS composite.

In the Bt spectrum, a prominent peak emerges from Al-OH at 915 cm^{-1}, accompanied by a robust peak at 1001 cm^{-1} attributed to the Si-O bond [16]. Notably, peaks at 3623 and 1633 cm^{-1} signify stretching vibrations of OH groups in H_2O and the deformation band of OH in the water retained within the silica matrix, respectively [17, 18].

In the standard SDS spectrum, stretching vibration peaks of CH_3 and CH_2 groups manifest at 2955 cm^{-1}, 2916 cm^{-1}, and 2849 cm^{-1}, alongside the characteristic absorption peak of the sulfate acid group at 1216 cm^{-1}. Additionally, a pronounced peak at 1467 cm^{-1} denotes the deformation band of C-H [19, 20].

The organo-bentonite spectra of Bt/SDS exhibit a slight shift in the vibration peak of the Si-O bond to 998 cm^{-1}, along with characteristic peaks of SDS at 1216 cm^{-1}, 2922 cm^{-1}, and 2852 cm^{-1}, suggesting an interaction between SDS and bentonite [21].

Figure 2b) depicts the distinct bands of the various film constituents without alterations in peak occurrences, indicating a lack of bands among the diverse $Bt/SDS/Stch$ constituents, possibly due to the limited amount of Bt employed.

3.3. DRX analysis

The X-ray diffraction patterns of Bt, SDS, and their three composites are illustrated in Fig. 3.

Bt displays its characteristic peak at $2\theta = 6.8°$, corresponding to the d_{001} basal reflection of the clay. This peak signifies a basal spacing of 12.99 Å, indicating intercalation with a monolayer of water. SDS XRD spectra exhibit

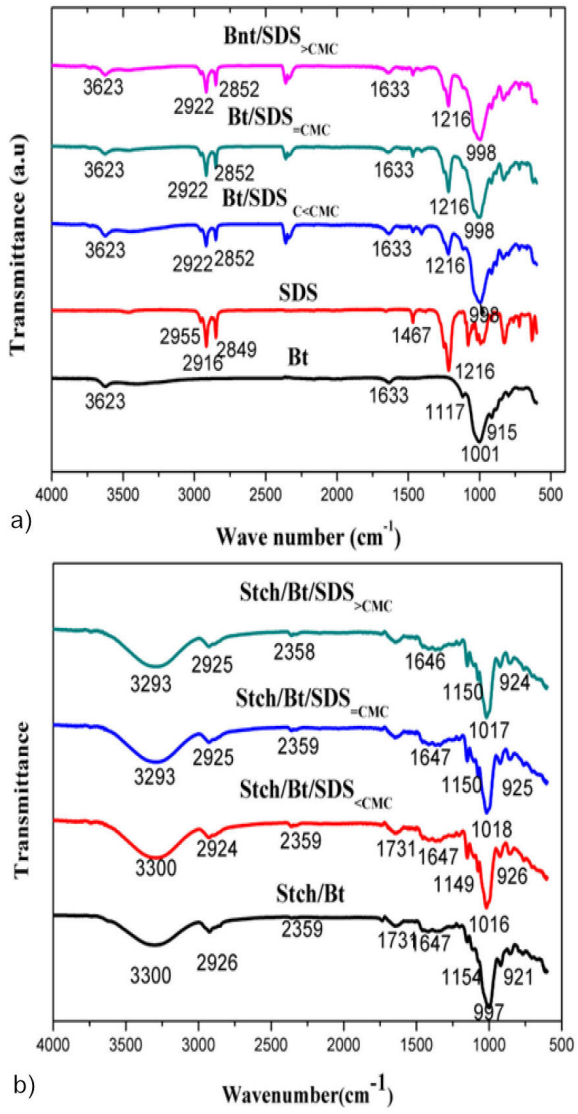

FIGURE 2. FTIR spectra of the Stch-based biofilm with the three SDS concentrations. a) $Stch/SDS$ b) $Stch/Bt/SDS$.

diffraction peaks at $2\theta = 2.406°$, $4.583°$, and $6.739°$. In the XRD pattern of the Bt/SDS composite, the typical Bt reflection ($2\theta = 6.8°$) vanishes, replaced by new group reflections. The first distance spacing ($2\theta = 6.35°$,$4.23°$, $2.172°$) of the composite with varying SDS concentrations results in values of 13.92 Å, 20.9 Å, and 40.65 Å, respectively, with a shift towards smaller angles for Bt/SDS at CMC. FTIR analysis suggests that SDS permeates the Bt layers, thereby expanding the interlayer space [22, 23]. These observations align with previous literature reports [24].

The distinctive peaks of the $Stch/Bt/SDS$ films at lower concentrations ($C < CMC$ and $C = CMC$) nearly vanish in Fig. 4, suggesting the presence of exfoliated nanostructures. This phenomenon aligns with previous studies [25, 26]. Conversely, concentrations exceeding the CMC reveal pronounced intercalation. Ideally, achieving perfectly

TABLE II. TGA of $Stch/Btand$ different $Stch/Bnt/SDS$ films-residual mass at different temperatures.

Temperature (°C)	$\%\,\Delta\, m\, Stch/Bt$	$\%\,\Delta\, m\, Stch/Bt/SDS_{<CMC}$	$\%\,\Delta\, m\, Stch/Bt/SDS_{=CMC}$	$\%\,\Delta\, m\, Stch/Bt/SDS_{>CMC}$
25-100	5.06	3.54	6.76	6.84
100-200	11.62	6.51	11.25	11.91
200-300	50.40	51.78	53.53	54.85
300-400	9.48	15.72	11.55	12.95
400-500	9.24	9.80	10.79	-
500-600	9.66	3.23	0.95	-

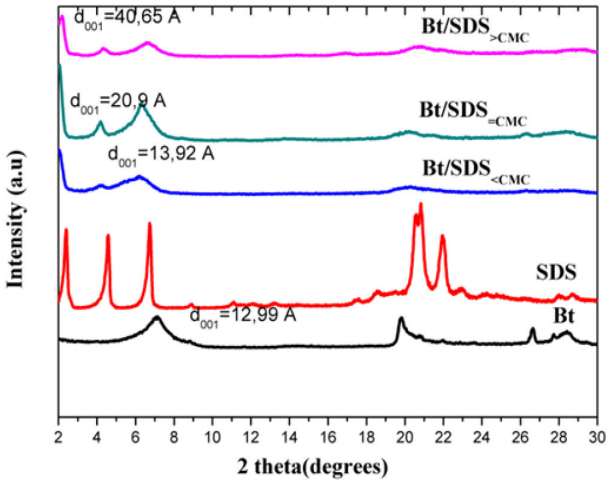

FIGURE 3. XRD patterns of Bt, SDS, $Bt/SDS_{<CMC}$, $Bt/SDS_{=CMC}$, $Bt/SDS_{>CMC}$.

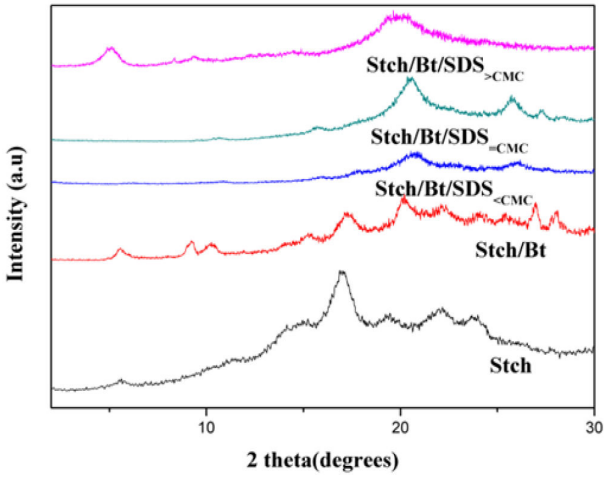

FIGURE 4. DRX patterns of $Stch$, $Stch/Bt$, $Stch/Bt/SDS_{<CMC}$, $Stch/Bt/\,SDS_{=CMC}$, $Stch/Bt/SDS_{>CMC}$.

intercalated or exfoliated nanostructures is necessary for enhancing the performance of polymer nanocomposites [27, 28].

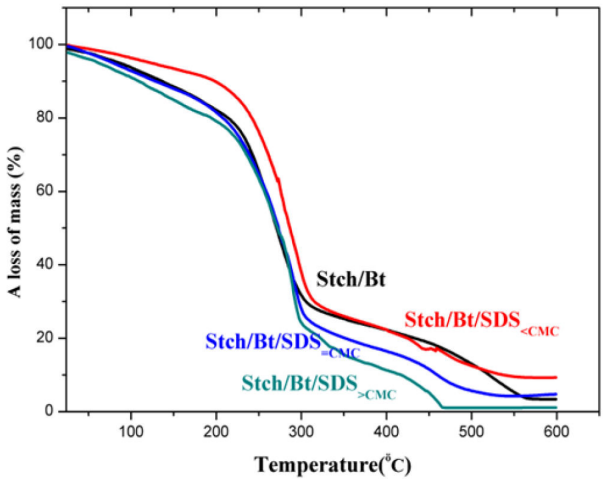

FIGURE 5. TGA curves of $Stch/Bt$, $Stch/Bt/SDS_{<CMC}$, $Stch/Bt/SDS_{=CMC}$, $Stch/Bt/SDS_{>CMC}$

3.4. TGA analysis

Thermogravimetric analysis (TGA) is an importante analytical technique for studying biofilms. It allows the determination of the thermal stability and composition of biofilms by measuring the variation in their mass as a function of temperature. This information is essential for understanding thermal degradation, decomposition processes, and the water and organic and inorganic content of biofilms.

In Fig. 5, all intervals have to be considered. Between 25°C and 200°C, for all three curves, there is a monotonous decrease in weight loss, suggesting the progressive release of water or volatile compounds present in the biofilm. The slight inflection point around 100°C could correspond to minor thermal transitions in the biofilm components, such as the desorption of adsorbed water or other volatile compounds [29].

Around 200°C, a sharp drop is observed in all three curves. This could indicate the beginning of thermal decomposition of the biofilm components, such as plasticized starch with glycerol, bentonite, and SDS. This abrupt drop suggests a significant transition in the thermal reactions of the biofilm [30, 31].

Between 200°C and 300°C, weight loss continues significantly in this temperature range. The higher the concen-

tration of SDS, the greater the weight loss appears to be. This could be due to a more significant decomposition of the biofilm components at higher concentrations of SDS [32].

Between 300°C and 450°C, the curve continues to decline, indicating ongoing decomposition of the remaining biofilm components. The observed difference in weight loss between different concentrations of SDS could reflect variations in the composition and thermal stability of the biofilm.

Above 450°C, the curves seem to reach a plateau, suggesting that the majority of the biofilm compounds have decomposedor volatilized. This plateau may indicate the presence of stableresidues or decomposition productsthat remain inthe system until higher temperatures [33].

These results show the influence of the concentration of SDS on the thermal decomposition of the biofilm, with higher concentrations of SDS leading to greater weight loss in the studied temperature range. This is due,to the SDS whose molecules are easily degradable.

3.5. Opacity and UV analysis

In essence, the intricate interplay between the internal and surface microstructure of a film plays a pivotal role in defining its optical properties, rendering the analysis of opacity a compelling metric for evaluating its suitability in packaging applications. Beyond mere optical considerations, such analysis serves as a window into the underlying structural nuances of film compositions. Moreover, the acknowledgment of thickness variations as a critical determinant of mechanical and barrier characteristics underscores the imperative of meticulous control over processing parameters to uphold quality standards. This holistic understanding, encapsulated in the comprehensive presentation of results in Table III, underscores the multifaceted nature of film assessment and its implications for diverse industrial applications.

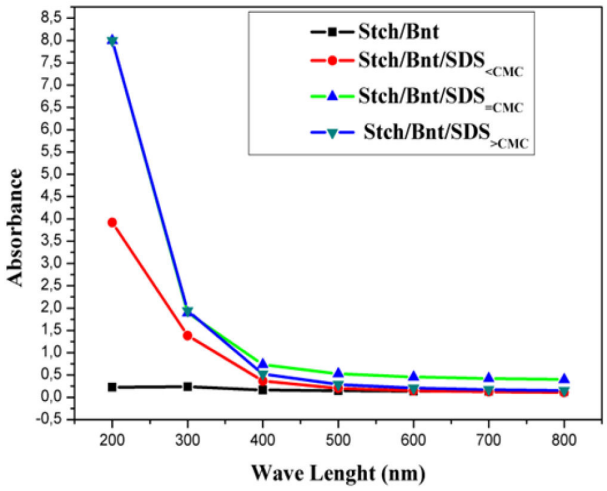

FIGURE 6. Films opacity of $Stch/Bt$, $Stch/Bt/SDS_{<CMC}$, $Stch/Bt/SDS_{=CMC}$, $Stch/Bt/SDS_{>CMC}$.

TABLE III. Measurements carried out for the four films studied.

The sample	Opacity	Thickness (mm)	Opacity/thickness (mm^{-1})
$Bt/Stch$	0.517	0.744	0.694
$Bt/SDS_{<CMC}/Stch$	0.343	0.426	0.805
$Bt/SDS_{=CMC}/Stch$	0.327	0.501	0.652
$Bt/SDS_{>CMC}/Stch$	0.213	0.544	0.393

Figure 6 presents the UV-visible absorbance spectra of two types of matrices: $Stch/Bt$ and $Stch/Bt/SDS$. The films used for these measurements were adjusted to a thickness ranging between 0.5 and 0.75 mm.

In the graph, we observe a slight alteration in the optical clarity of the Starch/Bentonite matrix film when SDS is introduced. With an increase in SDS concentration within the Starch/Bentonite matrix, there's a corresponding rise in absorbance across the visible UV spectrum [34]. Notably, the Starch/Bentonite/SDS matrix exhibits the highest absorbance within the 200-400 nm range compared to all other samples. This heightened absorbance can be attributed to the effective and uniform dispersion of the SDS surfactant within the Starch/Bentonite matrix [35].

3.6. SEM analysis

The dispersion and distribution of surfactants in composites, assessed via scanning electron microscopy (SEM), are vital for determining composite properties. SEM provides detailed images that show how uniformly the reinforcement material is spread and distributed within the polymer matrix.

Figure 7 presents images showcasing the morphological disparities between composites with and without SDS. Specifically, in images b) and c) spotlight the profound impact of compatibility and homogeneity on the properties of the films under investigation. It is noteworthy that any white spots observed in these images, such as spherical or lenticular shapes, represent starch granules stemming from the precipitation and fermentation process of the starch [36]. These observations provide valuable insights into the structural integrity and composition of the composites, elucidating key factors influencing their performance.

3.7. MOP analysis

To comprehensively analyze the morphology of the produced films, we employed optical measurements microscopy (MOP) to investigate how the addition of SDS affects the surface characteristics across varying SDS concentrations, as depicted in Fig. 8.

In Fig. 8, image a), clusters and aggregated particles are evident, likely stemming from the poorcompatibility of the Starch/Bentonite mixture. Conversely, images b and c vividly exhibit improved compatibility, indicative of the exfoliation effect, particularly noticeable at SDS concentrations less thanor equal to the critical micelle concentration (CMC) [37]. Figure 8d) presents a distinct appearance compared to

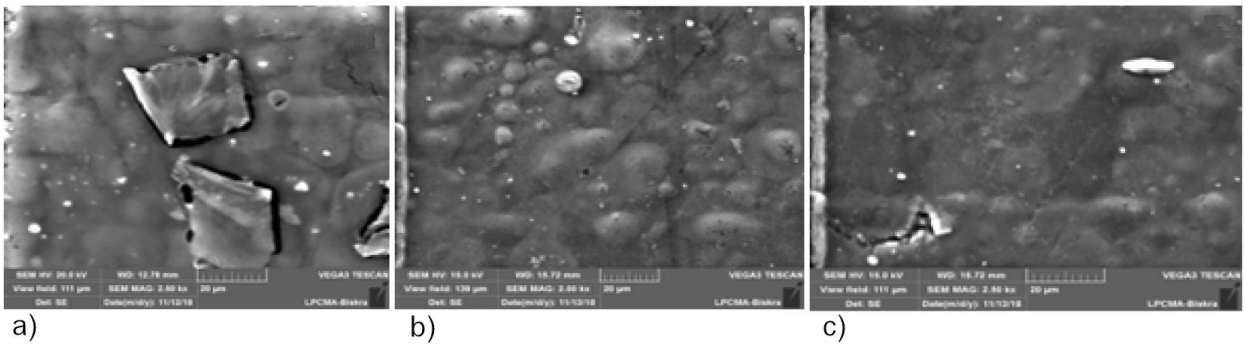

FIGURE 7. SEM images ofbased starch films with (a) $Stch/Bt$, (b) $Stch/Bt/SDS_{=CMC}$, (c) $Stch/Bt/SDS_{>CMC}$.

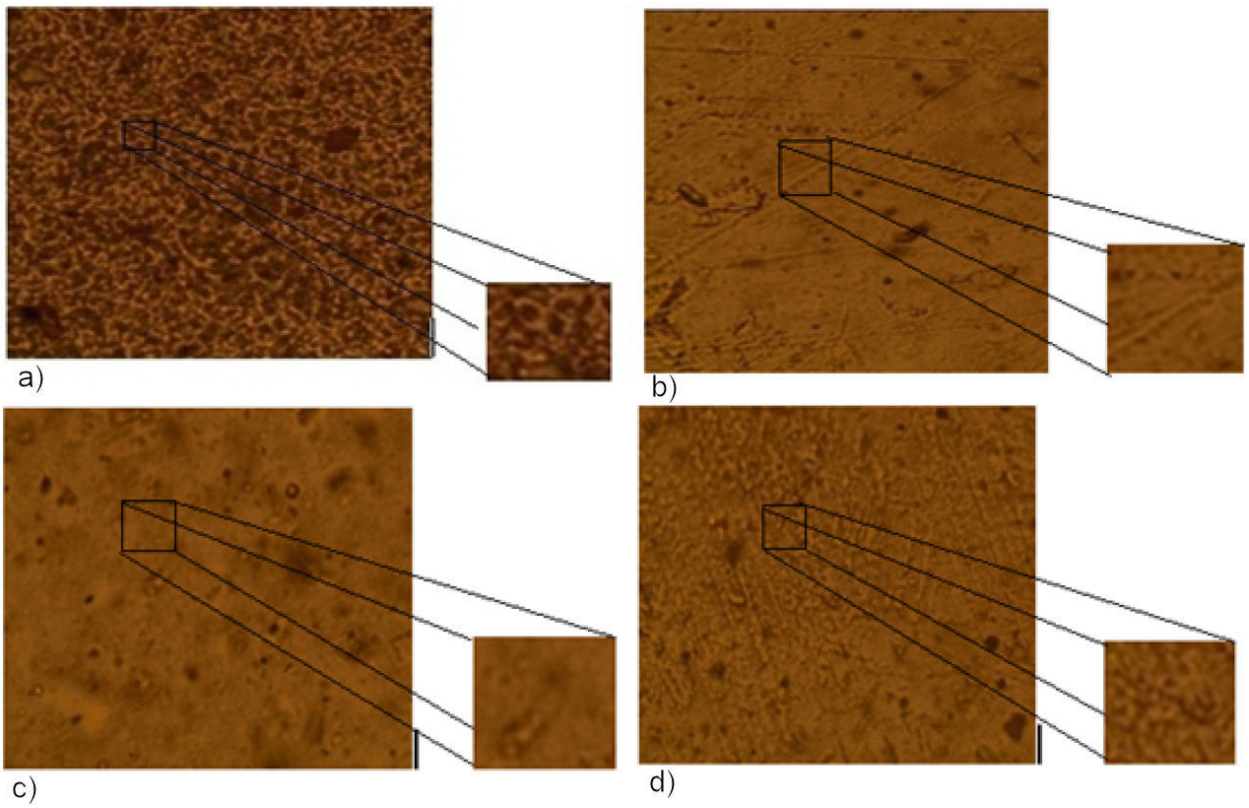

FIGURE 8. MOP images of based starch films with a) $Stch/Bt$, b) $Stch/Bt/SDS_{<CMC}$, c) $Stch/Bt/SDS_{=CMC}$, d) $Stch/Bt/SDS_{>CMC}$.

images a), b), and c), suggesting an intermediate level of compatibility, wherein strong intercalation of SDS within the Bentonite matrix is observed. These observations shed light on the nuanced interplay between SDS concentration and film morphology, providing valuable insights into the structural evolution of the composites [38].

4. Conclusion

In summary, this investigation underscores the pivotal role of sodium dodecyl sulfate (SDS) concentration in shaping the production and properties of biodegradable biofilms. Through an array of meticulous physico-chemical analyses, it elucidates the intricate interplay between SDS and the constituent elements of the biofilm, particularly starch and glycerol-plasticized bentonite. The findings reveal a nuanced relationship wherein low SDS concentrations facilitate exfoliation, while higher concentrations induce strong intercalation, resulting in notable enhancements in biofilm homogeneity. Microscopic observations and mass loss analyses further corroborate these insights, shedding light on the mechanisms underlying SDS-mediated degradation. Ultimately, this study not only underscores the significance of SDS concentration in biofilm production but also heralds promising avenues for the advancement of sustainable and eco-friendly materials.

1. E. Schwach, *Étude de systèmes multiphases biodégradables à base d'amidon de blé plastifié: relations structure-propriétés approche de la compatibilisation*, Thèse de doctorat, Université de Reims - Champagne Ardenne (2004).
2. A. Sandali, N. Rabhi, *Comportement au choc des stratifiés composites renforcés par des fibres naturelles*, Mémoire de master, Université Kasdi Marbah de Ouargla (2013).
3. P. Colonna, *La chimie verte*, (Lavoisier, Paris, 2005), ed. Tec & Doc.
4. A. Hebeish, A. A. Aly, A. El-Shafei, and S. Zaghloul, *Synthesis and characterization of cationized starches for application in flocculation, finishing and sizing*, Egyptian Journal of Chemistry, **52** (2009) 73, https://www.researchgate.net/publication/289228076.
5. H. Ismail, M. Irani, and Z. Ahmad, *Utilization of waste polystyrene and starch for superabsorbent composite preparation*, Journal of Applied Polymer Science, **127** (2012) 4195, https://doi.org/10.1002/app.37952.
6. H. Namazi and M. Mosadegh, *Preparation and properties of starch/nanosilicate layer/polycaprolactone composites*, Journal of Polymers and the Environment, **19** (2011) 980, https://doi.org/10.1007/s10924-011-0366-5.
7. M. Marcin, *Thermoplastic starch a green material for various industries*, In L. P. B. M. Janssen and L. Moscicki (Eds.), TPS and its nature (Wiley-Interscience, New York, 2009), pp. 77-104.
8. W. Amnuay and T. Sampan, *Sustainable green composites of thermoplastic starch and cellulose fibers*, Songklanakarin Journal of Science and Technology, **36** (2014) 149.
9. L. Qiu, F. Hu, and Y. Peng, *Structural and mechanical characteristics of film using modified corn starch by the same two chemical processes used in different sequences*, Carbohydrate Polymers, **91** (2013) 590, https://doi.org/10.1016/j.carbpol.2012.08.072.
10. H. L. Boudjemah, *Élaboration de matériaux composites biodégradables issus de ressources renouvelables*, Thèse de doctorat, Université d'Oran 2, Institut de Maintenance et de Sécurité Industrielle (2016).
11. L. Y. El Hadji Babacar, *Nouveaux matériaux composites thermoformables Ã base de fibres de cellulose*, Thèse de doctorat, Institut National Polytechnique de Grenoble (2008).
12. M. Mondragón, K. Arroyo, and J. Romero-García, *Biocomposites of thermoplastic starch with surfactant*, Carbohydrate Polymers, **74** (2008) 201, https://doi.org/10.1016/j.carbpol.2008.02.004.
13. B. Chen and J. R. G. Evans, *Thermoplastic starch-clay nanocomposites and their characteristics*, Carbohydrate Polymers, **61** (2005) 455, https://doi.org/10.1016/j.carbpol.2005.06.020.
14. A. Jiménez, M. J. Fabra, P. Talens, and A. Chiralt, *Edible and biodegradable starch films: A review*, Food and Bioprocess Technology, **5** (2012) 2058, https://doi.org/10.1007/s11947-012-0835-4.
15. Z. N. Ganga and H. Corke, *Physical properties of starch of Asian-adapted potato varieties*, Journal of the Science of Food and Agriculture, **79** (1999) 1642, https://doi.org/10.1002/(SICI)1097-0010(199909)79:12⟨1642::AID-JSFA412⟩3.0.CO;2-2.
16. D. Demirgoz, C. Elvirs, J. F. Mano, A. M. Cunha, E. Piskin, and R. L. Reis, *Chemical modification of starch-based biodegradable polymeric blends: Effects on water uptake, degradation behavior and mechanical properties*, Polymer Degradation and Stability, **70** (2000) 161, https://doi.org/10.1016/S0141-3910(00)00102-6.
17. M. Kim and S. J. Lee, *Characteristics of crosslinked potato starch and starch-filled linear low-density polyethylene films*, Carbohydrate Polymers, **50** (2002) 331, https://doi.org/10.1016/S0144-8617(02)00057-7.
18. M. I. Khalil and A. A. Aly, *Evaluation of some starch derivatives containing amide groups as flocculants*, Starch- Stärk, **53** (2001) 323, https://doi.org/10.1002/1521-379X(200107)53:7⟨323::AID-STAR323⟩3.0.CO;2-Z.
19. F. A. Aouada, L. H. C. Mattoso, and E. Longo, *New strategies in the preparation of exfoliated thermoplastic starch-montmorillonite nanocomposites*, Industrial Crops and Products, **34** (2011) 1502, https://doi.org/10.1016/j.indcrop.2011.05.003.
20. M. M. Hossain, M. I. H. Mondal, M. M. R. Khan, A. B. M. F. Al Am, and A. T. M. K. Hasan, *Interactions between starch and surfactants by ternary phase diagram*, *Canadian Journal on Scientific and Industrial Research*, **3** (2012) 246.
21. J. A. Mbey and F. Thomas, Components interactions controlling starch-kaolinite composite films properties, *Carbohydrate Polymers*, **1170** (2015) 739, https://doi.org/10.1016/j.carbpol.2014.10.053.
22. G. Zhuang *et al.*, *A new ball milling method to produce organo-montmorillonite from anionic and nonionic surfactants*, Applied Clay Science, **104** (2015) 18, https://doi.org/10.1016/j.clay.2014.11.023.
23. X. Cao, J.Wang, M. Liu, Y. Chen, Y. Cao, and X. Yu, Chitosancollagen/ organomontmorillonite scaffold for bone tissue engineering, *Frontiers in Materials Science*, **9** (2015) 405, https://doi.org/10.1007/s11706-015-0317-5.
24. Y. Gao *et al.*, *Effects of organic modification of montmorillonite on the performance of starch-based nanocomposite films*, Applied Clay Science, **99** (2014) 201, https://doi.org/10.1016/j.clay.2014.06.033.
25. S. Mohanty and S. K. Nayak, *Effect of clay exfoliation and organic modification on morphological, dynamic mechanical, and thermal behavior of melt-compounded polyamide-6 nanocomposites*, Polymer Composites, **28** (2007) 153, https://doi.org/10.1002/pc.20284.
26. F. Chivrac, E. Pollet, M. Schmutz, and L. Avérous, New approach to elaborate exfoliated starch-based nanobiocomposites, *Biomacromolecules*, **9** (2008) 896, https://doi.org/10.1021/bm7012668.

27. S. Pavlidou and C. D. Papaspyrides, *A review on polymer-layered silicate nanocomposites*, Progress in Polymer Science, **33** (2008) 1119, https://doi.org/10.1016/j.progpolymsci.2008.07.008.

28. Y. Xi, R. L. Frost, and H. He, *Modification of the surfaces of Wyoming montmorillonite by the cationic surfactants alkyl trimethyl, dialkyl dimethyl, and trialkyl methyl ammonium bromides*, Journal of Colloid and Interface Science, **305** (2007) 150, https://doi.org/10.1016/j.jcis.2006.09.033.

29. A. Pozsgay *et al.*, Gallery structure and exfoliation of organophilized montmorillonite: Effect on composite properties, *European Polymer Journal*, **40** (2004) 27, https://doi.org/10.1016/j.eurpolymj.2003.09.010.

30. A. Vazquez, M. López, G. Kortaberria, L. Martín, and I. Mondragon, *Modification of montmorillonite with cationic surfactants. Thermal and chemical analysis including CEC determination*, Applied Clay Science, **41** (2008) 24, https://doi.org/10.1016/j.clay.2007.10.001.

31. Z. B. Xu, W. W. Kong, M. X. Zhou, and M. Peng, Effect of surface modification of montmorillonite on the properties of rigid polyurethane foam composites, *Chinese Journal of Polymer Science*, **28** (2010) 615, https://doi.org/10.1007/s10118-010-9111-0.

32. Y. D. Wang, S. Zhang, C. L. Ma, and H. D. Li, *Synthesis and room temperature photoluminescence of ZnO/CTAB ordered layered nanocomposite with flake-like architecture*, Journal of Luminescence, **126** (2007) 661, https://doi.org/10.1016/j.jlumin.2006.10.018.

33. M. Babaee, M. Jonoobi, Y. Hamzeh, and A. Ashori, *Biodegradability and mechanical properties of reinforced starch nanocomposites using cellulose nanofibers*, Carbohydrate Polymers, **132** (2015) 1, https://doi.org/10.1016/j.carbpol.2015.06.043.

34. R. Bodirlau, C. A. Teaca, and I. Spiridon, *Influence of natural fillers on the properties of starch-based biocomposite films*, Composites Part B: Engineering, **44** (2013) 575, https://doi.org/10.1016/j.compositesb.2012.02.039.

35. S. C. Lara and F. Salcedo, *Gelatinization and retrogradation phenomena in starch/montmorillonite nanocomposites plasticized with different glycerol/water ratios*, Carbohydrate Polymers, **151** (2016) 206, https://doi.org/10.1016/j.carbpol.2016.05.065.

36. V. Vamadevan, E. Bertoft, Structure-function relationships of starch components, *Starch-Stärke*, **67** (2014) 55, https://doi.org/10.1002/star.201400188.

37. F. M. Pelissari, M. M. Andrade Mahecha, P. José, A. Sobral, and F. C. Menegalli, *Nanocomposites based on banana starch reinforced with cellulose nanofibers isolated from banana peels*, Journal of Colloid and Interface Science, **505** (2017) 154, https://doi.org/10.1016/j.jcis.2017.05.106.

38. M. I. H. Mondal, M. M. Hossain, and M. R. Sharif, *Study of starch-based biodegradable polymeric surfactants for better cleansing activity*, International Research Journal of Pure and Applied Chemistry, **4** (2014) 805, http://dx.doi.org/10.9734/irjpac/2014/10562.

39. J. A. Mbey, S. Hoppe, and F. Thomas, Cassava starch-kaolinite composite film: Effect of clay content and clay modification on film properties, *Carbohydrate Polymers*, **88** (2012) 213, https://doi.org/10.1016/j.carbpol.2011.11.091.